EUROPEAN ORGANIZATION FOR NUCLEAR RESEARCH (CERN)

CERN-PH-EP-20XX-YYY
LHCb-PAPER-20XX-YYY
February 10, 2016

The novel real-time alignment and calibration of the LHCb detector

Author list to be populated once we are closer to the end.

Abstract

We gonna do what they said can't be done...

Submitted to a journal with infinite impact factor

1 Introduction

For me we should have a different introduction 1) PID/Align performance needed to get optimal performance 2) Possibility to have in trigger together with a new strategy =¿ imply better ferformance RICH PID

The LHCb experiment is a single-arm forward spectrometer at the LHC. It has been designed as a dedicated heavy flavour physics experiment focused on the reconstruction of c and b hadrons. During Run 1 its physics programme has been extended to electroweak, soft QCD and even heavy ion physics. This was made possible in large part due to its versatile real-time reconstruction and analysis (trigger), which is responsible for reducing the rate of proton-proton collisions which need to be saved for offline analysis by approximately three orders of magnitude. LHCb's Run 1 trigger executed a simplified version of the full offline event reconstruction. Most charged particles above 300 MeV of transverse momentum were available to classify the event, and particle identification and the use of neutral particles such as photons or π^0 mesons was available on-demand to specific classification algorithms. Although this trigger enabled a great deal of LHCb's physics programme, the lack of very low momentum charged particles and full particle identification information limited the performance for c hadron physics in particular. In addition, resolution differences between the online and offline reconstructions led to difficulties in understanding efficiencies with a high degree of precision.

For these reasons, the LHCb trigger system was redesigned during the 2013-2015 long shutdown to perform the full offline event reconstruction, and the entire data processing framework was redesigned to enable a single, coherent, real-time detector alignment and calibration, as well as real-time analyses using information directly from the trigger system. The key objectives of this redesign were twofold : firstly to enable the full offline reconstruction to run in the trigger, greatly increasing the efficiency with which charm and strange hadron decays could be selected, and secondly to achieve the same alignment and calibration quality within the trigger as could be achieved offline in Run I, enabling the entire analysis to be performed at the trigger level.

In order to achieve this objective, the alignment and calibration of all the different components of the LHCb detector have been fully automated. Specific data streams are defined which supply each alignment and calibration algorithm with the events it needs, the algorithms themselves have been parallelized to enable them to run online within, for the most part, a matter of minutes, and a monitoring framework has been designed to ensure that any problems with alignment and calibration are spotted and rectified before they can affect data quality.

This paper describes the novel real-time alignment and calibration of the LHCb detector, to the best of our knowledge the first of its kind in High Energy Physics. Two companion papers describe the design and performance of the new uniform online-offline reconstruction sequence [] and the real-time analysis [] framework, which are made possible by the real-time alignment and calibration.

2 The LHCb detector

It is needed a more detailed detector description to be able to understand all the different alignment and calibration task description. To be see for example if in the detector peformance paper we have a better or more complete description.

The LHCb detector [1, 2] is a single-arm forward spectrometer covering the pseudorapidity range $2 < \eta < 5$, designed for the study of particles containing b or c quarks. The detector coordinate system is such that $\mathbf{z}$ is along the beamline and $\mathbf{x}$ is along the horizontal bending plane. The detector includes a high-precision tracking system consisting of a silicon-strip vertex detector (VELO) surrounding the pp interaction region [3]∗, a large-area silicon-strip detector located upstream of a dipole magnet with a bending power of about 4 Tm, and three stations of silicon-strip detectors (ST) and straw drift tubes [4]∗ (OT) placed downstream of the magnet. The tracking system provides a measurement of momentum, p, of charged particles with a relative uncertainty that varies from 0.5% at low momentum to 1.0% at 200 GeV/c. The minimum distance of a track to a proton-proton collision (primary vertex), the impact parameter, is measured with a resolution of $(15 + 29/p_{\mathrm{T}})\,\mu$m, where p_{T} is the component of the momentum transverse to the beam, in GeV/c. Different types of charged hadrons are distinguished using information from two ring-imaging Cherenkov detectors [5]∗. Photons, electrons and hadrons are identified by a calorimeter system consisting of scintillating-pad (SPD) and preshower detectors, an electromagnetic calorimeter and a hadronic calorimeter. Muons are identified by a system composed of alternating layers of iron and multiwire proportional chambers [6]∗. The LHCb detector datataking is divided into fills and runs. A fill is a single period of proton-proton collisions delimited by the announcement of stable beam conditions and the dumping of the beam by the LHC. A fill is subdivided into runs, each of which lasts a maximum of one hour.

Detector simulation has been used in the tuning of most reconstruction and selection algorithms discussed in this paper. In simulated LHCb events, pp collisions are generated using Pythia [7] with a specific LHCb configuration [8]. Decays of hadronic particles are described by EvtGen [9], in which final-state radiation is generated using Photos [10]. The interaction of the generated particles with the detector, and its response, are implemented using the Geant4 toolkit [11] as described in Ref. [12].

3 Datataking Strategy

A schematic diagram showing the trigger data flow in Run 2 is depicted in Figure 1. The maximum rate at which events can be read out of the detector is imposed by the front-end electronics and corresponds to a rate of 1.1 MHz. In order to determine which events are kept, hardware triggers based on field-programmable gate arrays are used with a fixed latency of 4 μs. Information from the ECAL, HCAL, and muon stations is used in separate `L0` triggers. Events selected by `L0` are transferred to the High Level Trigger (HLT) for further analysis and selection.

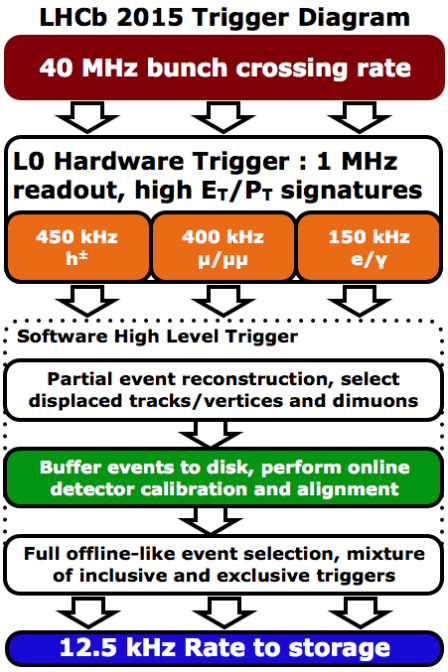

Figure 1: Trigger strategy for Run II: after the hardware stage and a first software stage based on a partial reconstruction, the selected events are buffered on disk while the real-time calibration and alignment are performed. The second stage of the software trigger performs the same reconstruction performed offline using the same calibration and alignment.

The HLT is divided into two stages, HLT1 and HLT2, processed on an Event Filter Farm (EFF) of approximately 1700 nodes with 27000 physical cores, which allows to simultaneosuly run 50000 processes using hyper-threading technology. Events selected by an HLT1 trigger are buffered to the local harddisk of each node before being processed by HLT2. This buffering is done for two purposes : events can be processed during inter-fill periods, and the detector can be calibrated and aligned run-by-run before the HLT2 stage. During 2012 LHC spent only approximately 30% of its time in stable running due to e.g. planned technical stops, machine developement phases and the time between data taking fills needed for the ramping of the LHC dipole magnets. The usage of the local disks, around 5 PBytes in total, allows around 150 hours of LHC datataking to be buffered, and has enabled LHCb to fully utilize the EFF throughout the tecnical stops and machine development phases (with the exception of the annual winter shutdown of the LHC), more than doubling the effective available processing power. It is this buffering which allows the full offline event reconstruction to be executed in the HLT2 stage.

The HLT1 trigger performs an inclusive selection of events based on one or two track combinations, the presence of muon tracks displaced from the primary vertex, or dimuon combinations in the event. Crucially, it is also able to select the types of events required by each alignment and calibration task, and these events are flagged by specific routing bits which allow them to be streamed to the relevant tasks. There are two kinds of alignment and calibration tasks : those which are expected to change for each run, and those which are expected to change less frequently, perhaps once per fill or once every few fills. In the first case, which mainly concerns the calibration of the RICH detectors, the calibration constants are calculated for each run and updated before the HLT2 processing of that run. In the second case, the alignment and calibration constants are calculated for each run,

and an automated monitoring task checks if they have changed by more than a certain threshold with respect to the previous values. When such a significant variation is observed, a change of run is triggered. The new constants are updated for the new run to be used online by the two stages of the software trigger, and offline, for every further reconstruction and selection. As these variations are infrequent and slow, the events collected in the run preceeding this update are still reconstructed in HLT2 and offline with the same constants used by HLT1. Once the detector is fully aligned and calibrated the events are processed by HLT2, where a full event reconstruction is performed.

This strategy has several advantages: firstly it minimises the difference between the online and offline performance, allowing a more effective trigger selection that can take advantage of the hadron identification information. For example charm physics is limited by trigger output rate contraints; using hadron identification in the trigger allows to have a higher selection efficiency and purity for the doubly Cabibbo suppressed modes and, at the same time, satisfy the output rate constraints by pre-scaling the more abundant Cabibbo favourite modes. Secondly it ensures the stability of the alignment quality and hence of the physics performance. Finally, as in Run II the last level of the trigger performs the same reconstruction as the one performed offline, it will be possible to run some physics analyses, with the same offline performance, directly on the output of the trigger using the special stream of data known as Turbo stream [**?**]. This approach has the advantage that, for some events, it will be possible to save only the information on the signal candidate tracks ($\sim$ 5 kB per event) instead of all the electronic signals recorded from the detector ($\sim$ 70 kB per event). This decrease of more than one order of magnitude of the event size will allow a higher selection rate, for example in the charm analyses that during Run I used trigger lines which were pre-scaled due to output rate requirements. It is obvious that the real-time alignment and calibration becomes essential when the raw event is not saved.

4 The Physics Impact of Alignment and Calibration

Importance of alignment and of rich pid selection (example run1). To be included also effect of alignment on ip resolution. To be added also something about the calorimeter calibration.

The spatial alignment of a detector and the accurate calibration of its subcomponents are essential to achieve the best physics performance. The correct alignment of the VELO is needed to identify primary vertices and secondary vertices from the decay of particles containing b or c quarks while a misalignment of the tracking system would degrade the momentum and mass resolution. Figure 2 shows how an improved alignment greatly enhances the Υ mass resolution from 92 MeV/c^2 with the first alignment to 49 MeV/c^2 with the improved one.

An exclusive selection using hadron identification criteria relies on the complete calibration of the ring-imaging Cherenkov detectors. Figure 3 shows the effect in the $B^0 \to h^+h^-$ mass spectrum of hadron identification criteria: the ratio between the signal, $B^0 \to \pi^+\pi^-$, and the combinatorial background increases by approximately a factor two and the ratio

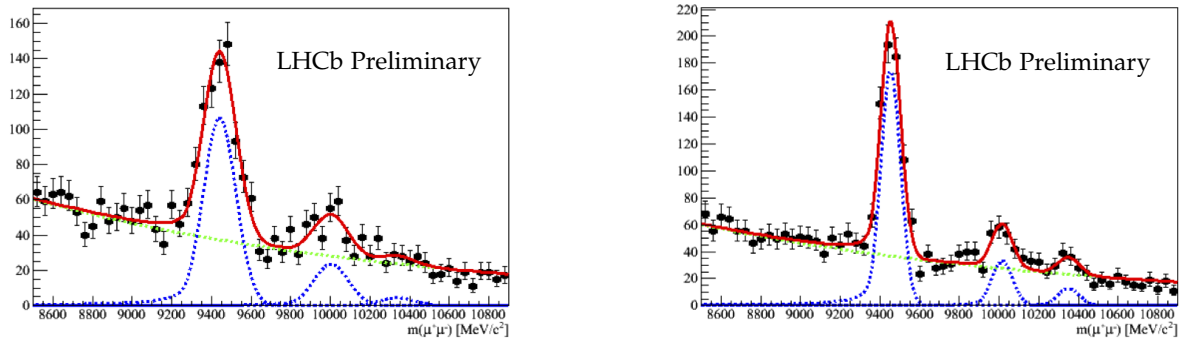

Figure 2: Invariant mass distribution for $\Upsilon \to \mu\mu$. The mass resolution is 92 MeV/c^2 with the first alignment (left) and is enhanced to 49 MeV/c^2 with an improved alignment (right).

between the signal and the favoured $B^0 \to K\pi$, increases by a factor 35.

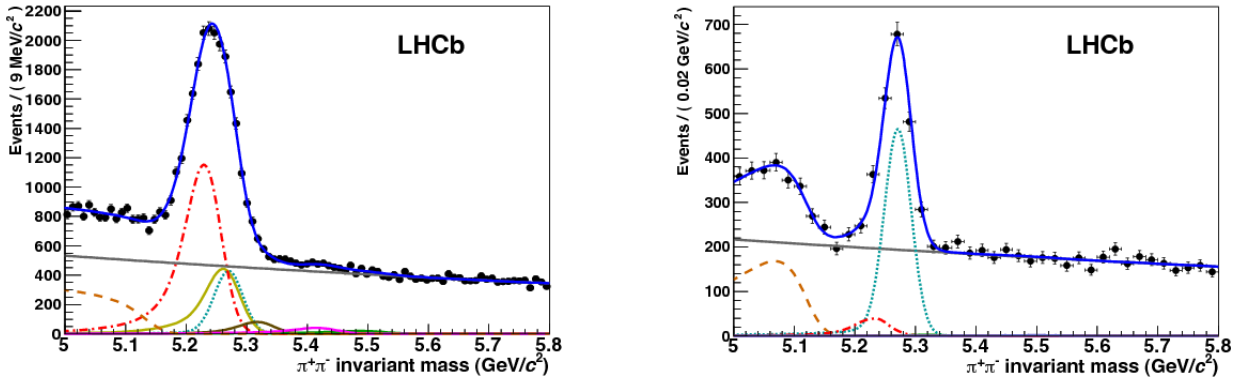

Figure 3: Invariant mass distribution for $B^0 \to h^+h^-$ decays [13] in the LHCb data before the use of the RICH information (left), and after applying RICH particle identification (right). The signal under study is the decay $B^0 \to \pi^+\pi^-$, represented by the turquoise dotted line. The contributions from different b-hadron decay modes ($B^0 \to K\pi$ red dashed-dotted line, $B^0 \to$ 3-bodies orange dashed-dashed line, $B_s \to KK$ yellow line, $B_s \to K\pi$ brown line, $\Lambda_b \to pK$ purple line, $\Lambda_b \to p\pi$ green line), are eliminated by positive identification of pions, kaons and protons. Only the signal and two background contributions remain visible after applying hadron identification requirements. The grey solid line is the combinatorial background.

Is it thus clear that using a real-time alignment and calibration during the trigger selection allows a higher signal purity and a more effective selection on the channels interesting to pursue LHCb's physics program without increasing the overall trigger rate. This, however, requires us to align more than 1700 detector components and compute almost 2000 calibration constants in real-time. It is therefore important to understand the frequency with which the relevant constants are expected to vary.

The VELO is made of two halves that during the data taking are at approximately 8

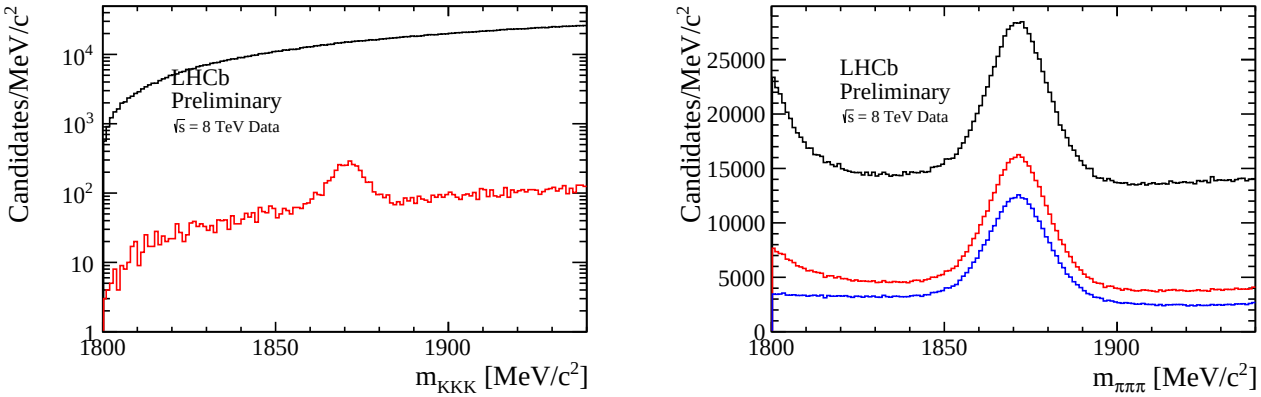

Figure 4: 3 body decay distribution for D0 to kkkk (left) and pipipi (right). To be written

mm away from the nominal beam position. For the safety of the detector during the beam injection at the beginning of a fill the halves are retracted by 29 mm; when stable beam is declared the VELO is closed around the beam. The VELO halves are moved using stepper motors and their position is read from resolvers mounted on the motor axes with an accuracy better than 10 μm. An automated closing procedure positions the VELO halves around the beams using the response of the hardware and the measured positions of the beams. By considering the two independent beam profiles compiled by each half, the VELO is observed to close symmetrically around the beams to an accuracy of better than 4 μm. As the VELO is closed for each fill, its alignment may change with the same frequency.

Figure 5 shows for a subsample of the Run I dataset the variation of the misalignment between the two halves in the horizontal direction perpendicular to the beam. It can be estimated by taking the difference of the positions of the primary vertices reconstructed separately with tracks in only one half of the VELO. In a perfectly aligned detector the mean of this difference should be zero. The average variation in Run I is $\sim 4\,\mu$m while the maximum variation is $O(10\,\mu\text{m})$, which is more than the $O(2\,\mu\text{m})$ precision of the track based software alignment procedure [3].

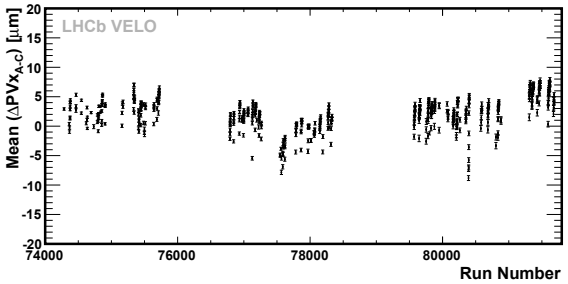

Figure 5: Misalignment between the two VELO halves along the main movement direction for the different runs, evaluated by fitting the primary vertices separately with tracks in each half of the VELO. The run numbers shown here span the period of the last four months of operations in 2010.

For the other components of the tracking system, in addition to the variation due to

hardware intervention, some variation over time was observed, partially correlated to the magnet polarity which is reversed periodically. During Run I a new tracking alignment has been evaluated after each magnet polarity switch or technical stop. This strategy allowed to have a momentum scale and resolution stable with time as shown in Figure 6.

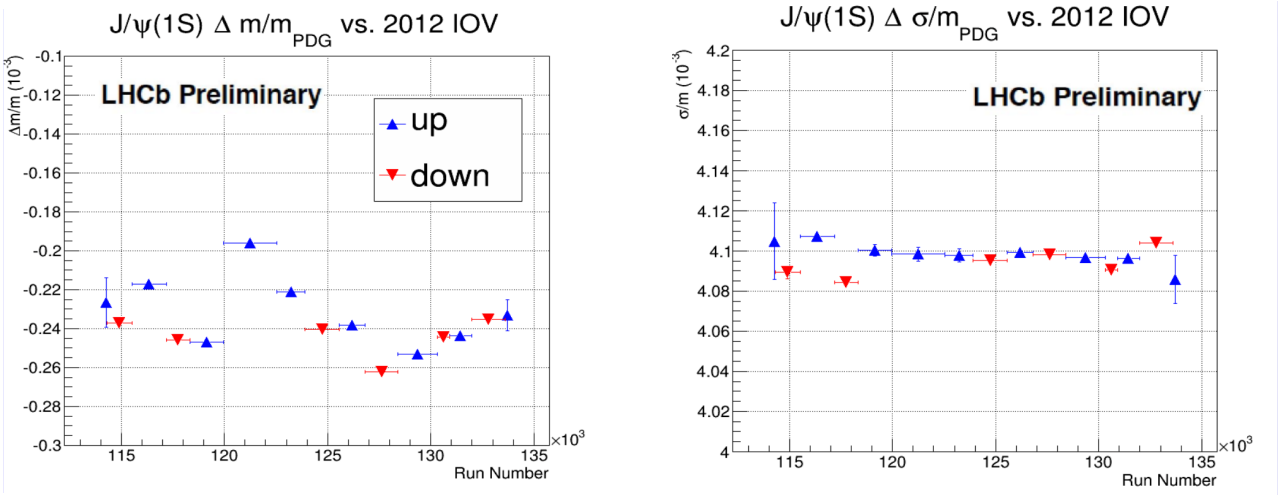

Figure 6: Time evolution of the relative variation of the difference between the measured mass of the $J/\Psi(1S)$ and the nominal one from [**?**] (left) and relative variation of the mass resolution at the $J/\Psi(1S)$ mass (right). Each point corresponds to data taken with a different tracking alignment; the blue up-triangles and red down-triangles correspond to opposite magnet polarities.

Finally, in the case of the gaseous RICH detectors, the variations of temperature and pressure in the experimental cavern mean that the refractive index of the gas changes continuously. In order to achieve the best particle identification performance, it is necessary to compute these constants for each run. On the other hand, the alignment of the RICH mirrors is seen to vary only infrequently, and in general only needs to be updated after an extended shutdown of the detector. **DO WE HAVE SOME JUSTIFICATION?**

SAY SOMETHING ABOUT THE EXPECTED VARIATION OF THE CALO HERE?

5 The Online Alignment Framework

To allow the calibration and alignment tasks to operate, they have been embedded in the online system in terms of data flow and control flow.

5.1 Data Flow

All of the tasks make use of events that have been accepted by the HLT1 stage of the High Level Trigger. The alignment tasks require events with specific content such as decays of $D^0 \to K\pi$ or $J/\psi \to \mu^+$ µm, or tracks with specific properties. The calibration tasks have

no requirements on the event content, but do require a sufficient number of events to fill the distributions used to obtain the calibration constants.

Events for the alignment tasks are selected by dedicated selections that are part of HLT1 and, based on acceptance by these selections, written to files on the hard-drives installed in the farm nodes. The number of events written to files across the farm is tracked and once a sufficient number for a given task has been accumulated, the tasks writing events are stopped, until a new sample is required. The Velo alignment requires

Approximately a kilohertz of events accepted by HLT1 is transferred over the network to dedicated tasks that processes as many of these events as they can. These tasks provide the distributions required to perform the calibration, and write them to files. The files are written every fifteen minutes and at least once per run, which is a period of data-collection up to an hour long.

5.2 Control Flow

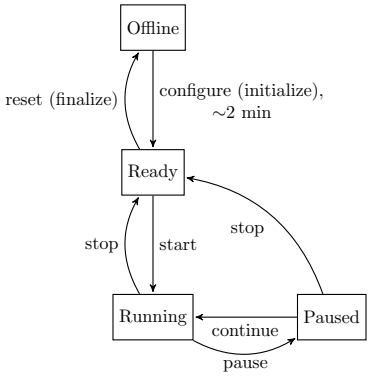

Figure 7: Finite state machine that defines the behaviour of the alignment tasks.

The Outer Tracker calibration and RICH refractive index calibration tasks run independently from ECS and wait for the files containing the distributions they require. Once a file becomes available for a given run, the calibration algorithms are triggered to process the distributions, and if a new set of calibration constants is created, write these to a file. The ECS is then informed of the availability of the new versions and which run(s) these correspond to.

The execution of the alignment tasks is under the control of the LHCb Experiment Control System (ECS), and is implemented as a finite state machine, which is shown in fig. 7. Once FSM reaches the initial "READY" state, it will loop from "READY"→"RUNNING"→"PAUSED"→"READY" until it stops when a convergence criterium is satisfied.

The task that steers the iterations is called the iterator and the tasks that analyze the data are called the analyzers; both tasks follow the same sequence of states. When all tasks are in the "READY" state, the iterator makes an initial set of alignment constants

available to the analyzers and then updates its state to "RUNNING". The analyzers are then sent the "start" command, update their state to "RUNNING" and start analyzing their data. Each analyzer that has completed processing its data updates its state to "PAUSED", and once they have all reached this state, they are sent the "stop" command and update their state to "READY". The iterator is then sent the "pause" command, collects and combines the output produced by the analyzer tasks and either indicates that conversion has been reached by updating its state to "READY", or that further iteration is required by producing a new set of constants and updating its state "RUNNING". If the iterator decides that the process has converged and the changes in the alignment constants are above a given threshold, it writes the new alignment constants to a file and announces the new version to the control system.

6 Alignment and Calibration Tasks

7 Alignment and Calibration Tasks

7.1 Tracking Alignment

7.1.1 Alignment method

give more details

The tracking alignment is based on an iterative procedure where the residuals of a Kalman track fit are minimised. The magnetic field and material effects are taken into account and information from vertices and particle masses can also be used as constraints to avoid global distortions [**?**, **?**].

Given a set of tracks reconstructed using the alignment parameters α_0, the new set of alignment constants can be found solving the system of equations

$$\alpha = \alpha_0 - \left(\frac{d^2\chi^2}{d\alpha^2}\right)^{-1}\Bigg|_{\alpha_0} \frac{d\chi^2}{d\alpha}\Bigg|_{\alpha_0}, \tag{1}$$

where the derivatives of the total χ^2 with respect to the alignment parameters are obtained by summing the contributions from all the tracks:

$$\begin{aligned} \frac{d\chi^2}{d\alpha} &= 2 \sum_{\text{tracks}} \frac{dr}{d\alpha}^T V^{-1} r, \\ \frac{d^2\chi^2}{d\alpha^2} &= 2 \sum_{\text{tracks}} \frac{dr}{d\alpha}^T V^{-1} R V^{-1} \frac{dr}{d\alpha}. \end{aligned} \tag{2}$$

Here V is the covariance matrix of the measurement coordinates, r is the track residuals (the distance between the hit position and the track intercept point), and R is the covariance matrix of the residuals. It is assumed that the χ^2 has been minimised with respect to the track parameters for the alignment α_0.

7.1.2 VELO Alignment

it should include (random order):stability plots, variation of the constants, time needed to run the jobs, event selections. Performance before/aftera alignment. Trend of the constants and evaluation of the variation. Maybe trends of physics quantity like mass or time resolution

7.1.3 Tracker Alignment

7.1.4 Muon Alignment

7.2 RICH Mirror Alignment

This should include, description of the method (detector description should be included in previous section), data selected, time required for this task, performance (before/after alignment) and stability of the constants. The overall performance, maybe also stability of the overall performance (PID or/and cherenkov angle resolution) could be together for calibration and alignment.

Both RICH detectors have two sets of mirrors: photons are reflected off a primary mirror onto a secondary mirror, from where they are deflected out of the LHCb acceptance onto the photodetector plane.

Any misalignment of the RICH detectors with respect to the tracking system is observed as a shift of the track projection point on the photodetector plane from the center of its corresponding Cherenkov ring as is illustrated in Figure 8. This shift is observed by analysing the Cherenkov angle, θ, as a function of the azimuthal Cherenkov angle ϕ, defined as the angle of the pixel hit in the coordinate system of the photodetector plane, with the projected track coordinate at the origin. For a well aligned detector the angle θ is independent of the angle ϕ, whilst a misaligned system results in a sinusoidal distribution as shown in Figure 9.

In practice, distributions of $\Delta\theta$ against ϕ are plotted for each possible combination of primary and secondary mirror, where $\Delta\theta(\phi) = \theta(\phi) - \theta_{\rm Ch}$ and $\theta_{\rm Ch}$ is the Cherenkov angle calculated from the momentum of the track and the refractive index of the radiator [5]. Any systematic shift away from the value $\theta_{\rm Ch}$ is observable as a shift in $\Delta\theta$.

The $\Delta\theta$ distribution is then divided into slices in ϕ. For each slice, a one dimensional histogram of $\Delta\theta$ is fitted with a Gaussian plus a second order polynomial background, where the means of the Gaussians of the different slices are connected in the fit by a sinusoidal distribution given by

$$\begin{aligned} \Delta\theta_{p,s}(\phi) &\equiv [\theta(\phi) - \theta_{\rm Ch}]_{p,s} \\ &= \Theta^{z}_{p,s}\cos\phi + \Theta^{y}_{p,s}\sin\phi \end{aligned} \tag{3}$$

The final fit is shown in Figure 9; the extracted values of $\Theta^{y}_{p,s}$ and $\Theta^{z}_{p,s}$ correspond to the misalignment on the photodetector plane for a mirror combination of primary mirror p and secondary mirror s in the y and z direction respectively.

The alignment of the mirror segments has the extra complication that every photon is

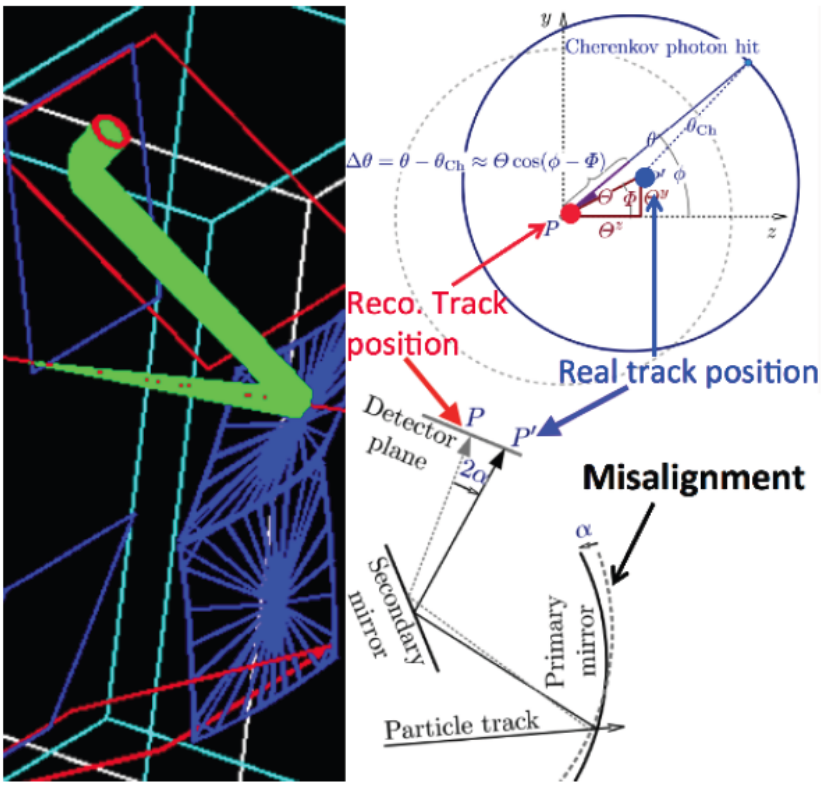

Figure 8: Left: 3D representation of a track (red line) going through a radiator and emitting Cherenkov photons (green cone). The photons are reflected by a spherical primary mirror (blue rectangle with star-shaped pattern) onto a flat secondary mirror (blue rectangle) and from there onto the photodetector plane (red rectangle). The observable Cherenkov ring is shown as a red circle on the photodetector plane. Right: Schematic illustration of the effects of a misalignment in the RICH mirror system. The projected track position on the photodetector plane P is displaced by Θ^z and Θ^y with respect to the the actual center of the Cherenkov ring on the photodetector plane P'. The Cherenkov angle θ is evaluated relative to P and varies with the azimuthal angle ϕ.

reflected twice, and thus the data must be separated into samples which have unique primary and secondary mirror combinations. For this procedure, only photons that can be uniquely associated to a given mirror combination are used.

The mirror arrangement in RICH1 allows for alignment using a sequential approach, where the primary mirrors are aligned first, followed by the secondary mirrors. This is possible because photons reaching a particular secondary mirror can only be reflected from a single primary mirror. In RICH2 the larger number of primary/secondary mirror combinations makes the use of a sequential method impossible. The alignment of the RICH2 mirror segments is performed by solving a set of simultaneous equations to extract all the alignment parameters of all the mirrors. In general two iterations of this method

are required to obtain the final mirror alignment.

As for the tracker alignment, the RICH1 and RICH2 alignments are performed

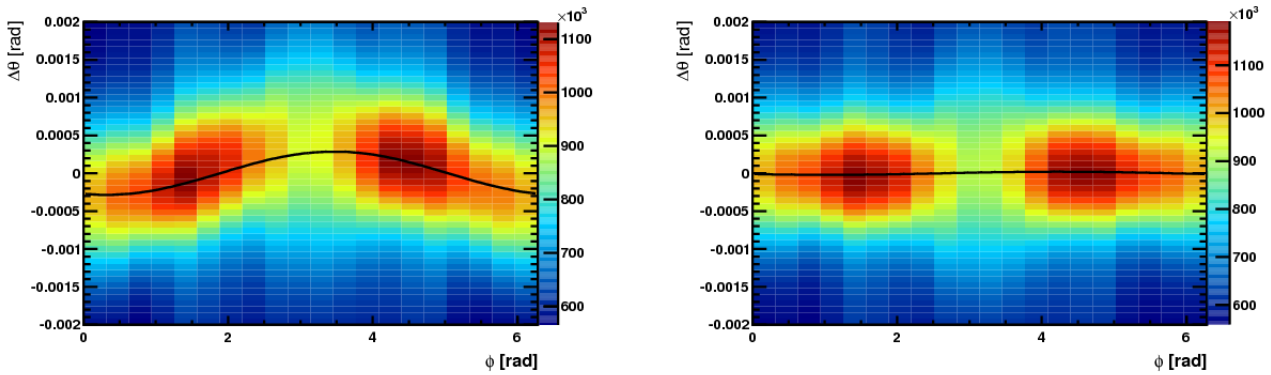

Figure 9: Difference between the measured and expected Cherenkov angle $\Delta\Theta$ as a function of the azimuthal angle ϕ before (left) and after (right) the mirror alignment for one mirror [5].

on events collected by their respective HLT1 lines. The HLT1 lines for the RICH alignments trigger on high energy tracks whose Cherenkov photons would populate the outermost mirror combinations. The other mirror combinations are populated by the other tracks in the events. All tracks entering the alignment procedure have to have a momentum p greater than 20(40) GeV for RICH1 (RICH2) in order for the Cherenkov angle to be saturated and therefore θ_{Ch} be predictable from the track momentum and the refractive index of the radiator.
The event reconstruction and filling of the $\Delta\theta$ vs. ϕ histograms is done by the analysers in parallel. The individual histograms are collected and merged and then fitted by the iterator. The iterator also determines the individual mirror misalignments and creates a new database slice with the mirror orientations and decided weather the alignment procedure has converged or if another iteration needs to be started. The alignment procedure takes about XXX for RICH1 and XXX for RICH2.
MORE ON STABILITY AND PERFORMANCE TO COME SOON.

7.3 Rich Calibration

This should include, description of the method (detector description should be included in previous section), data selected, time required for this task, performance (before/after calibration) and stability of the constants or variation as function of temperature/pressure. The overall performance, maybe also stability of the overall performance (PID or/and cherenkov angle resolution) could be together for calibration and alignment.

The RICH automatic calibration consists of calibrating the RICH refractive index and the Hybrid Photon Detectors (HPDs) images. Both these calibrations are evaluated and updated every run.

The refractive index of the gas radiators depends on the ambient temperature and pressure, and the exact composition of the gas mixture and so can change in time. These quantities are monitored to compute an expected refractive index, but this does not have a high enough precision and needs to be corrected. The distribution of the difference between the reconstructed and expected Cherenkov angle is fitted to extract the scale factor to correct the expected refractive index.

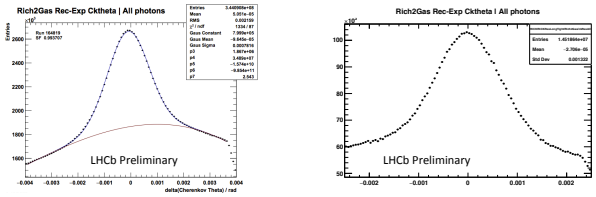

Figure 10: RICH cherenkov angle before (left) and after (right) the calibration,Caption to be written, 1st draft for the plot

HPDs are used to detect Cherenkov photons. They consist of vacuum tubes separated from the radiator gas by a quartz window and a photocathode. The photoelectrons produced are focused onto a silicon pixel array using an accelerating voltage [5]. The anode images are affected by magnetic and electric fields, and so are cleaned and a Sobel filter [**?**] is used to detect the edges. Figure 10 shows the anode images before and after this process. The evaluation of the new calibration constants does not require an iterative procedure and can be obtained by fitting the relevant distribution on a single node.

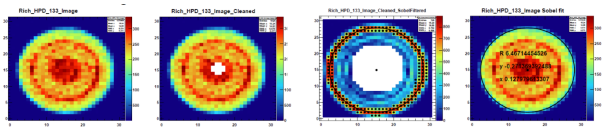

Figure 11: RICH HPD anode images,Caption to be written, 1st draft for the plot.

7.4 OT Calibration

The LHCb Outer Tracker (OT) [4] is a detector consisting of gas-filled straws with a 5 mm pitch. The time difference between a bunch crossing and the measurement of a signal in one of the straws, t_{meas}, consists of several compenents as expressed by:

$$t_{\text{meas}} = t_0 + t_{\text{flight}} + t_{\text{prop}} + t_{\text{drift}}, \tag{4}$$

where t_0 is the time delay caused by the readout electronics, t_{flight} is the time-of-flight of the charged particle that caused the signal, t_{prop} is the time required for the signal to propagate along the wire to the readout electronics, and t_{drift} the drift-time of electrons in the gas.

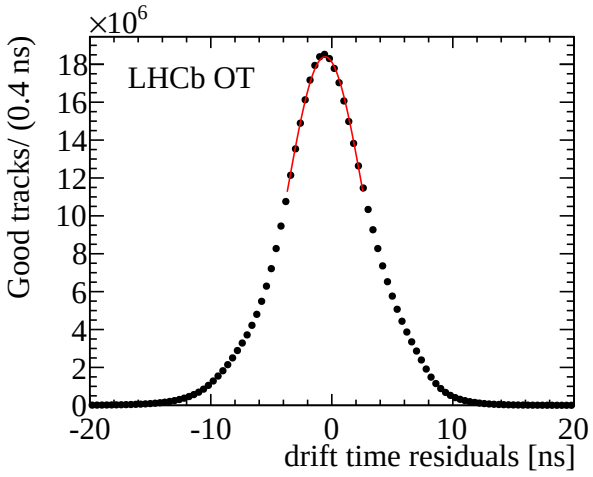

Figure 12: Fit to the distribution of the drift-time residuals of Outer Tracker hits, used to estimate the global time offset between the collision time and the LHC clock.

While the t_0 time delay is different for each read-out board of the OT, it can be written as the sum of a average, detector-wide, offset and a per-board offset. As the per-board offsets are a property of the electronics, they are expected to change very little. The global offset changes more frequently as a result of, for example, drift of the arrival time of the LHC clock to which the readout is synchronised. To correct for these global clock changes, a near-realtime analysis is performed to calibrate it.

Data accepted by the HLT1 stage of the HLT is sent to a small farm running of $O(50)$ of the LHCb reconstruction application, Brunel. Good quality tracks that traverse the Velo and OT are selected and the expected drift-times of hits in the OT are calculated from the track parameters. The residual differences between the expected and measured drift-times are entered into a histogram and a fit of a Gaussian function to the central part of the resulting distribution is performed to extract the global offset. An example of such a fit it shown in fig. 12.

Data is collected in LHCb in periods of up to an hour long, called runs. The calibration is performed at most once per run once a distribution of drift-time residuals of sufficient size has been obtained; fifty thousand entries are typically sufficient. The task that performs the calibration waits for the distribution of drift-time residuals to be made available to it, which occurs approximately every fifteen minutes, and at the end of a run. The calibration is then performed and if the difference with the last known best calibration is larger than a threshold, the new calibration is saved and automatically propagated to all tasks running online at the start of the next run; it is also inserted into the database used by tasks running offline. Figure 13 shows the values of the global time offset obtained during July and August of 2015.

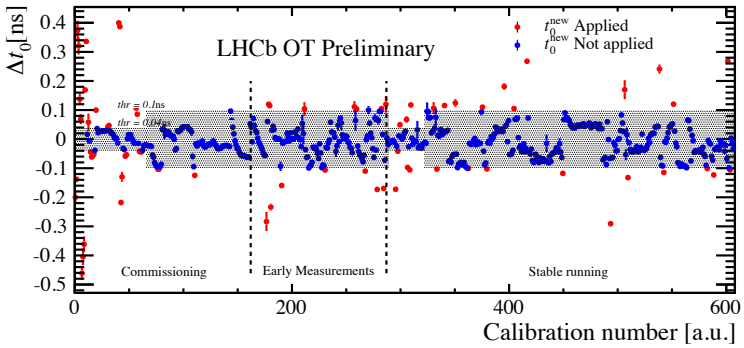

Figure 13: Global t_0 values obtained by the calibration task over time. Red points indicate values that were above threshold and therefore propagated to online and offline tasks and databases.

7.5 Calorimeter Calibration

In order to have a constant L0 rate the calorimeter gain should not change with time. The variation of the gain can be estimated by the variation of the relative occupancy. The occupancy for a cell is defined as the fraction of events in which the ADC output is above a threshold. The ratio of the occupancies with respect to a reference sample is proportional to the changes in gain. A relative calibration is performed online on a single node for each fill using this occupancy method and when needed the high voltage is changed accordingly.

An absolute calibration can be obtained with the π^0 method: the reconstructed π^0 mass can be determined for each cell by fitting di-photon mass distributions where one of the photon has the cell as the seed. The calibration coefficients can be tuned to constrain the reconstructed π^0 mass to the nominal one. This fine calibration requires an iterative procedure and it is run on the HLT farm similarly to the tracking or RICH mirror alignment. This second method takes several hours to run and will be performed a few times per year i.e. during technical stops.

7.5.1 Calibration with Relative Occupancy and LEDs

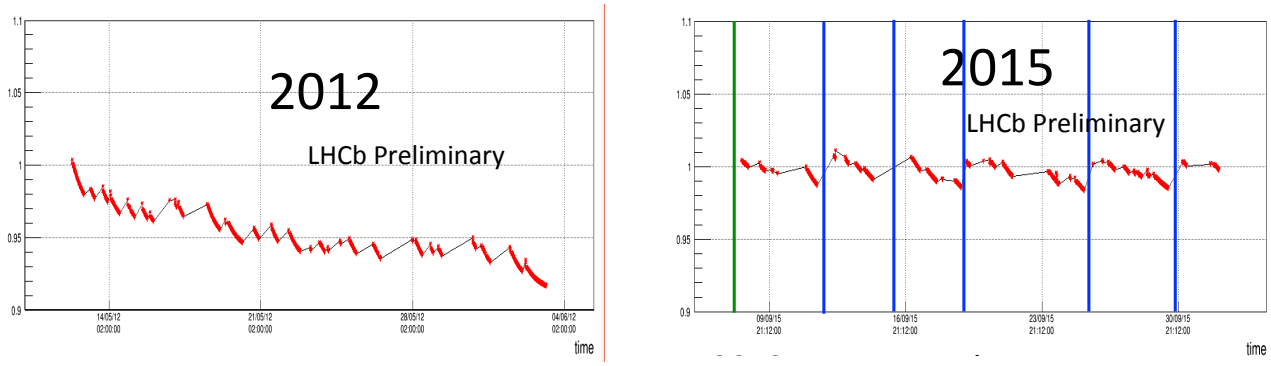

Figure 14: Stability of calorimeter calibration. Caption to be written, 1st draft for the plot

Task	Used by
Velo alignment	HLT1, HLT2 and offline
tracker alignment	HLT1, HLT2 and offline
muon alignment	L0 Muon and monitoring
ECAL calibration	update of ECAL high voltages
RICH mirror alignment	HLT2 and offline
RICH calibrations	HLT2 and offline
OT calibration	HLT1, HLT2 and offline

Table 1: Processing phases or detector systems that require the result of calibration and alignment tasks.

7.5.2 Absolute Calibration for HCAL with Cs source

7.5.3 Absolute Calibration for ECAL with π^0

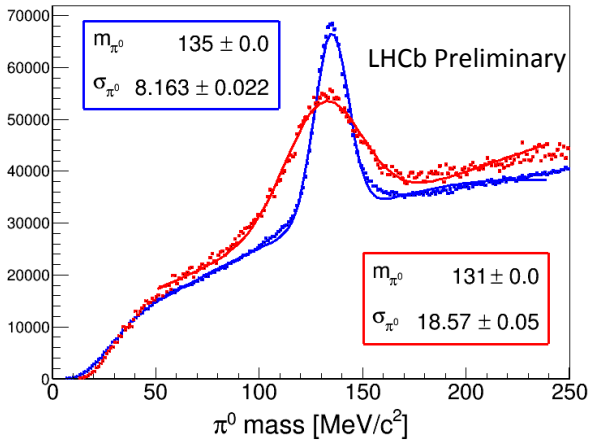

Figure 15: Stability of calorimeter calibration. Caption to be written, 1st draft for the plot

8 Scheduling

Give an overview of the scheduling for all the tasks: at beginning of each fill? each 1 week? when we update constants/hv/ if trigger run change. Some details could/should included in each section but probably it would be good to have some 'overview' of the schedule.

9 Propagation of Constants

Once a calibration or alignment task has completed, it writes the constants it produced to one or more XML file. To allow propagation of these constants to the data processing

tasks, such tasks have been configured to read relevant calibration and alignment constants from these XML files. Whenever a task receives an event that belongs to a new data taking period, a new set of XML files is read to obtain the latest constants.

Table 1 gives on overview of where constants are used. The different phases where constants are needed broadly fall into three categories: HLT1, HLT2 and offline; HLT2 and offline; and detector subsystems. If constants are used in HLT1, HLT2 and offline, they are used across all of these phases starting from a fixed point in time after the result has been obtained. This usually means the start of the next data-taking period of up to an hour. If constants are not needed in HLT1, but only by HLT2 and offline, HLT2 will not start processing data from a given data-taking period until the constants for that data-taking period have been produced. Results of tasks used only by subsystems are interpreted by subsystem experts and used to make updates to the configuration of those system if and when required.

If constants are needed for offline processing, they are added to the conditions database as soon as all constants for a given data taking period are available. Once the constants have been added to the conditions database, a cross-check is performed by configuring one task to read the constants from the XML files, another task to read them from the conditions database, and comparing the constants they obtain. If any mismatches are detected, the corresponding data taking period is not declared ready for offline processing. Experts then investigate the source of the mismatches and resolve the problem.

10 Benefits to Physics

textcolorredmaybe here more on trigger efficiency or put here high level quantity like mass or time or pid..... to be decided. When the different sections are ready we can decide if we want to move some performance in this section.

How this reflects in "physics" (comparison run1/run2 or with/without the update alignment/calibration)
for example the rate of the D-¿Kpipipi
stability of mass plot? or PV resolution? or proper time/ip chi2/ ip?
systematic? due to online/offline difference or alignment variation (efficiency or ip selection or difference acceptance online/offline)

11 Conclusion

In Run II the new scheme for the software trigger at LHCb allows the alignment and calibration to be performed in real time. A dedicated framework has been put in place to parallelise the alignment and calibration tasks on the multi-core farm infrastructure used for the trigger in order to meet the computing time constraints. Data collected at the start of the fill are processed in a few minutes and the output is used to update the alignment, while the RICH calibration constants are evaluated for each run. The same

framework is used to perform finer calibration less frequently and to monitor the alignment quality of various subdetector. This procedure allows a more stable alignment quality, more effective trigger selections and online-offline consistency thanks also to the same online-offline reconstruction. Physics analysis can be performed directly on the trigger output with the same online-offline performance.

Acknowledgements

The text below are the acknowledgements as approved by the collaboration board. Extending the acknowledgements to include individuals from outside the collaboration who have contributed to the analysis should be approved by the EB. The extra acknowledgements are normally placed before the standard acknowledgements, unless it matches better with the text of the standard acknowledgements to put them elsewhere. They should be included in the draft of first circulation.

We express our gratitude to our colleagues in the CERN accelerator departments for the excellent performance of the LHC. We thank the technical and administrative staff at the LHCb institutes. We acknowledge support from CERN and from the national agencies: CAPES, CNPq, FAPERJ and FINEP (Brazil); NSFC (China); CNRS/IN2P3 (France); BMBF, DFG, HGF and MPG (Germany); INFN (Italy); FOM and NWO (The Netherlands); MNiSW and NCN (Poland); MEN/IFA (Romania); MinES and FANO (Russia); MinECo (Spain); SNSF and SER (Switzerland); NASU (Ukraine); STFC (United Kingdom); NSF (USA). The Tier1 computing centres are supported by IN2P3 (France), KIT and BMBF (Germany), INFN (Italy), NWO and SURF (The Netherlands), PIC (Spain), GridPP (United Kingdom). We are indebted to the communities behind the multiple open source software packages on which we depend. We are also thankful for the computing resources and the access to software R&D tools provided by Yandex LLC (Russia). Individual groups or members have received support from EPLANET, Marie Skłodowska-Curie Actions and ERC (European Union), Conseil général de Haute-Savoie, Labex ENIGMASS and OCEVU, Région Auvergne (France), RFBR (Russia), XuntaGal and GENCAT (Spain), Royal Society and Royal Commission for the Exhibition of 1851 (United Kingdom).

References

[1] LHCb collaboration, A. A. Alves Jr. *et al.*, *The LHCb detector at the LHC*, JINST **3** (2008) S08005.

[2] LHCb collaboration, R. Aaij *et al.*, *LHCb detector performance*, Int. J. Mod. Phys. **A30** (2015) 1530022, arXiv:1412.6352.

[3] R. Aaij *et al.*, *Performance of the LHCb Vertex Locator*, JINST **9** (2014) P09007, arXiv:1405.7808.

[4] R. Arink *et al.*, *Performance of the LHCb Outer Tracker*, JINST **9** (2014) P01002, arXiv:1311.3893.

[5] M. Adinolfi *et al.*, *Performance of the LHCb RICH detector at the LHC*, Eur. Phys. J. **C73** (2013) 2431, arXiv:1211.6759.

[6] A. A. Alves Jr. *et al.*, *Performance of the LHCb muon system*, JINST **8** (2013) P02022, arXiv:1211.1346.

[7] T. Sjöstrand, S. Mrenna, and P. Skands, *PYTHIA 6.4 physics and manual*, JHEP **05** (2006) 026, arXiv:hep-ph/0603175; T. Sjöstrand, S. Mrenna, and P. Skands, *A brief introduction to PYTHIA 8.1*, Comput. Phys. Commun. **178** (2008) 852, arXiv:0710.3820.

[8] I. Belyaev *et al.*, *Handling of the generation of primary events in Gauss, the LHCb simulation framework*, J. Phys. Conf. Ser. **331** (2011) 032047.

[9] D. J. Lange, *The EvtGen particle decay simulation package*, Nucl. Instrum. Meth. **A462** (2001) 152.

[10] P. Golonka and Z. Was, *PHOTOS Monte Carlo: A precision tool for QED corrections in Z and W decays*, Eur. Phys. J. **C45** (2006) 97, arXiv:hep-ph/0506026.

[11] Geant4 collaboration, J. Allison *et al.*, *Geant4 developments and applications*, IEEE Trans. Nucl. Sci. **53** (2006) 270; Geant4 collaboration, S. Agostinelli *et al.*, *Geant4: A simulation toolkit*, Nucl. Instrum. Meth. **A506** (2003) 250.

[12] M. Clemencic *et al.*, *The LHCb simulation application, Gauss: Design, evolution and experience*, J. Phys. Conf. Ser. **331** (2011) 032023.

[13] LHCb collaboration, R. Aaij *et al.*, *Measurement of b-hadron branching fractions for two-body decays into charmless charged hadrons*, JHEP **10** (2012) 037, arXiv:1206.2794.